Authigenic iron oxide proxies for marine zinc over geological time and implications for eukaryotic metallome evolution

Leslie J. Robbins[1*], Stefan V. Lalonde[2], Mak A. Saito[3], Noah J. Planavsky[4], Aleksandra M. Mloszewska[1], Ernesto Pecoits[1], Clint Scott[5], Christopher L. Dupont[6], Andreas Kappler[7] and Kurt O. Konhauser[1]

1. Department of Earth & Atmospheric Sciences, University of Alberta, Edmonton, AB, Canada
2. UMR 6538 Domaines Océaniques, European Institute for Marine Studies, Technopôle Brest-Iroise, Plouzané, France
3. Marine Chemistry and Geochemistry Department, Woods Hole Oceanographic Institution, Woods Hole, MA, USA
4. Department of Earth Sciences, University of California, Riverside, Riverside, CA, USA
5. Department of Earth and Planetary Sciences, McGill University, Montreal, QC, Canada
6. Microbial and Environmental Genomics Group, J. Craig Venter Institute, San Diego, CA, USA
7. Geomicrobiology Group, Center for Applied Geoscience, University of Tuebingen, Tuebingen, Germany

Keywords: paleomarine zinc; metallome evolution; metalloenzymes; eukaryotic evolution; iron formations.

*Corresponding author: L.J. Robbins, Tel: 1-780-492-6532, fax: 1-780-492-2030, email: lrobbins@ualberta.ca

Abstract

Here we explore enrichments in paleomarine Zn as recorded by authigenic iron oxides including Precambrian iron formations, ironstones and Phanerozoic hydrothermal exhalites. This compilation of new and literature-based iron formation analyses track dissolved Zn abundances and constrain the magnitude of the marine reservoir over geological time. Overall, the iron formation record is characterized by a fairly static range in Zn/Fe ratios throughout the Precambrian, consistent with the shale record (Scott et al., 2013, Nature Geoscience, **6**, 125-128). When hypothetical partitioning scenarios are applied to this record, paleomarine Zn concentrations within about an order of magnitude of modern are indicated. We couple this examination with new chemical speciation models used to interpret the iron formation record. We present two scenarios: first, under all but the most sulfidic conditions and with Zn binding organic ligand concentrations similar to modern oceans, the amount of bioavailable Zn remained relatively unchanged through time. Late proliferation of Zn in eukaryotic metallomes has previously been linked to marine Zn biolimitation, but under this scenario, the expansion in eukaryotic Zn metallomes may be better linked to biologically intrinsic evolutionary factors. In this case zinc's geochemical and biological evolution may be decoupled, and viewed as a function of increasing need for genome regulation and diversification of Zn-binding transcription factors. In the second scenario, we consider Archean organic ligand complexation in such excess that it may render Zn bioavailability low. However, this is dependent on Zn organic ligand complexes not being bioavailable, which remains unclear. In this case, although bioavailability may be low, sphalerite precipitation is prevented, thereby maintaining a constant Zn inventory throughout both ferruginous and euxinic conditions.

50 These results provide new perspectives and constraints on potential couplings between
51 the trajectory of biological and marine geochemical coevolution.
52
53 **Introduction**
54 Zinc is the most common inorganic co-factor in eukaryotic metalloenzymes (Berg and
55 Shi, 1996; Maret, 2001; Dupont et al., 2010), and as a consequence, it has become the
56 basis for a hypothesis that the biological use of Zn may have evolved in the late
57 Precambrian when it became available in seawater (Williams and da Silva, 1996; Dupont
58 et al., 2006; 2010; Saito et al., 2003). Modern marine phytoplankton differ significantly
59 in their ability to grow at low Zn concentrations; modern surface seawater has
60 concentrations that range from ~0.04-0.5 nM (e.g. Bruland, 1989; Lohan et al., 2002).
61 Studies of marine cyanobacteria have found little to no measurable Zn requirement under
62 the conditions tested thus far in the globally abundant *Prochlorococcus* and
63 *Synechococcus* (Sunda and Huntsman 1995; Saito et al., 2002). In contrast, eukaryotic
64 phytoplankton have been observed to be quite sensitive to low zinc conditions. Some,
65 notably neritic diatoms (those that inhabit shallow marine waters from the littoral zone to
66 the edge of the continental shelf), are more sensitive and experience growth rates that are
67 significantly reduced at free Zn^{2+} concentrations below $10^{-11.5}$ M, while others show only
68 minor reductions in growth rates at 10^{-13} M (Brand et al., 1983). The centric diatom
69 *Thalassiosira* sp. displays dramatically reduced growth rates in coastal species at Zn
70 concentrations of $10^{-12.5}$ M (Tortell and Price, 1996); however, species from offshore
71 oligotrophic environments, such as *Thalassiosira oceanica*, are more tolerant of low Zn
72 conditions (Sunda and Huntsman, 1995). The unicellular algae, *Emiliania huxleyi* (a

coccolithopharad), shows decreased levels of alkaline phosphatase activity as Zn approaches picomolar concentrations (Shaked et al., 2006). Concentrations are low enough in modern environments that Zn stimulation or co-limitations of marine phytoplankton communities have been observed in some high nutrient, low chlorophyll environments (Franck et al., 2003; Jakuba et al., 2012), but not other environments (Crawford et al., 2003; Coale et al., 2005). While physiological studies of phytoplankton Zn requirements are limited and it is apparent that no single dissolved Zn concentration can be pinpointed as universally limiting, it is also apparent that severely suppressed marine Zn concentrations would have significant consequences for the activity and abundance of modern eukaryotic phytoplankton.

Such may have been the case in deep geological time. A survey of physiological experiments found that marine prokaryotic microbes, particularly the cyanobacteria, show metal nutritional requirements consistent with hypothesized Precambrian seawater compositions (Saito et al., 2003). From this it was suggested that during much of the Precambrian, the bioavailable marine Zn reservoir, as well as those of Cu and Cd, may have been much lower than in the modern oxygenated ocean due to the formation of strong aqueous complexes between Zn and sulfide that are likely not bioavailable (Luther et al., 1996; Edgcomb et al., 2004). Proteomic-based phylogenetic analyses also indicate a relatively late origin for most Zn-binding domains in eukaryotic metalloenzymes, leading to the suggestion that in addition to depressed oxygen availability, marine Zn biolimitation stemming from higher Precambrian sulfide concentrations and expanded euxinia during the mid-Proterozoic (1800 to 800 Ma) may have impeded eukaryotic diversification (Dupont et al., 2006; 2010). Accordingly, seemingly rapid eukaryotic

diversification in the Neoproterozoic (1000 to 542 Ma) may, in part, be tied to an enhanced bioavailable marine Zn reservoir accompanying oxygenation of the oceans. This model provides a simple link between the enigmatic and protracted diversification of eukaryotes and the shifting availability of bio-essential metals in a manner akin to a 'bio-inorganic bridge' (Anbar and Knoll, 2002).

However, until recently this possibility has yet to be evaluated in light of sedimentary proxies for the evolution of the paleomarine Zn reservoir. A recent examination of the shale record (Scott et al., 2013) indicates that Zn may have been near modern abundances and was likely bioavailable to eukaryotes throughout the Precambrian, casting doubt on the coupled geochemical and eukaryotic evolutions with respect to Zn utilization. Here, guided by new chemical speciation models, we explore eukaryotic evolution as revealed by a ~3.8 billion year record of marine authigenic iron oxide deposition, in the form of Precambrian iron formations, Phanerozoic ironstones and Fe-rich exhalites, herein collectively referred to as iron formations (IF). We use the rock record to shed light on the poorly understood relationships between marine trace metal availability, metalloenzyme proliferation, and biological innovation.

Zn is predominantly bound by organic ligands in modern seawater (e.g., Crawford et al., 2003), but it also occurs in aqueous form, i.e., Zn^{2+}, $Zn(OH)^{+}$, $Zn(OH)_2$, $ZnCO_3$, $ZnSO_4$, and $ZnCl_2$, suspended solids (e.g., ZnS), or adsorbed onto particle (e.g., Zirino and Yamamoto, 1972). Furthermore, Zn may be strongly complexed by aqueous sulfide (Luther et al., 1996) such that in anoxic environments, where HS^- is present, inorganic bisulfide and potentially polysulfide Zn complexes may play key roles in dominating the speciation of dissolved Zn (e.g., Gardner, 1974). Luther et al. (1999) provide an example

of when polysulfides may become dominant, which occurs when 10 μM Zn is titrated with sulfide in excess of 5 μM. In some conditions where a strong redoxcline exists, such as Jellyfish Lake, Palau (Landing et al., 1991), total dissolved Zn concentrations may actually increase at depth due to the formation of aqueous sulfide complexes. The proportion of Zn that is bioavailable is controlled by either sulfide complexation (Luther et al., 1996; Edgcomb et al., 2004) or by organic ligand complexation. However, complicating the issue of bioavailability is recent evidence that suggests organic complexation of Zn may in fact increase the potential for uptake (Aristilde et al., 2012).

In surface layers of the open ocean, horizontal and vertical mixing, atmospheric fallout, biological uptake, and particulate removal are the main controls on Zn abundance (Bruland, 1980). Accordingly, total dissolved Zn follows a nutrient profile in the modern oceans, where Zn is between ~0.04-0.5 nM in the surface layers, increasing below the photic zone to ~8-10 nM, where it remains relatively constant down to the seafloor (Bruland et al., 1994; Lohan et al., 2002; Nolting and de Baar, 1994). Despite this variability, for the purposes of discussion we assume a concentration of 10 nM as a "modern" value effectively describing the majority of the water column. While uptake in the photic zone could have lead to surface-deplete nutrient-type Zn depth profiles in the deep past, especially if concentrations were limiting, the Zn concentration of deep waters obviously plays an important role in the upward diffusive resupply of Zn (John, 2007) and thus upper water column Zn concentrations.

In terms of the modern zinc budget, inputs from mid-ocean ridge hydrothermal systems (~4.4×10^9 mol/yr) dominate riverine fluxes (~3.4×10^8 mol/yr) by a factor of 13, while diffuse off-axis venting contributes little marine Zn (~1×10^6 mol/yr)(Wheat et al.,

142 2002). However, the efficiency of scavenging of hydrothermal zinc is poorly constrained.
143 Modern aeolian Zn deposition is significant (~0.7 – 3.5x10^9 mol/yr), although roughly
144 75% is anthropogenic (Duce et al., 1991). Modern sinks are poorly constrained but likely
145 include organic matter, metal hydroxides, and sulfide burial fluxes. Modern hydrothermal
146 fluids, the primary natural Zn input, are enriched by 16,000 - 88,000 times the seawater
147 Zn value at their source (Doe, 1994), but these values drop significantly with distance
148 from the vent due to seawater dilution and Zn incorporation into sulfide and metal
149 hydroxide phases (Trocine and Trefry, 1988; German et al., 1991). Given higher mantle
150 recycling rates (e.g., Sleep and Windley, 1982), we consider a hydrothermal Zn
151 component to be more relevant during the Precambrian. Under anoxic and ferruginous
152 (Fe-rich) seawater conditions, with Fe(II)>S(-II) as required for iron(III) oxyhydroxide
153 formation, it is likely that hydrothermal Zn would have dispersed over wider areas of the
154 deep ocean for a lack of an effective sink, with a spatial distribution and areal extent
155 similar to Fe in the case of Precambrian iron formations (e.g., 10^6 km^2 in the Hamersley
156 basin; Morris, 1993).

157 Based on the low solubility of Zn sulfide minerals and the formation of strong
158 aqueous Zn-S complexes, expanded euxinia during the late Paleoproterozoic and
159 Mesoproterozoic has been proposed to have limited the bioavailability of Zn and other
160 sulfide-reactive trace metals (e.g., Cu, Cd), and thereby influenced metallome evolution
161 (Williams and Da Silva, 1996; Sunda and Huntsman, 1995; Saito et al., 2003). However,
162 recent work suggests that Proterozoic oceans were almost certainly laterally
163 heterogeneous in their geochemical characteristics (e.g., Planavsky et al., 2011), such that
164 sulfidic conditions may have been limited to shallow or coastal areas (e.g. Poulton et al.,

2010). Such considerations therefore warrant a re-examination of trace metal evolution in the context of a dominantly ferruginous Proterozoic ocean, especially with regards to elements vital for eukaryotic evolution such as Zn. Precambrian authigenic iron oxides, comprising laterally extensive IF that are highly Fe-rich and S-poor, necessitate Fe-rich and sulfide-poor conditions at the time of their deposition (Klein, 2005; Bekker et al., 2010). In this regard, the Precambrian IF record may be considered to represent large areas with conditions where Fe(II)>>S(-II). Such chemical deposits thus record ancient seawater where no strong euxinic metal sink was locally present; this makes the IF record an ideal target for exploring paleomarine concentrations of Zn.

Methods

Geochemical equilibrium calculations (Fig. 1) were performed using Visual MINTEQ 3.0 (Gustafsson, 2011) and the primary thermodynamic database provided (thermo.vdb) was modified to account for multiple aqueous Zn sulfide complexes as well as Zn complexation by organic ligands (SI Table 1). Modeling conditions included seawater-like salinity (0.56 M NaCl), standard temperature (25ºC), the exclusion of molecular O_2 and a pCO_2 of 10 times present atmospheric levels (PAL). Calcium, pH and Fe were determined by equilibrium reactions with excess calcite and siderite. Redox considerations were omitted such that all Fe and S species are +II and –II, respectively. Supersaturated minerals were permitted to precipitate and activity corrections were made using the Davies equation. Figure 1 presents chemical equilibrium models of speciation in the Fe(II)-S(-II)-Zn-organic-ligand system in terms of molar concentrations and mineral saturation indices (IAP/K_{sp}) and as a function of increasing total system sulfide

188 concentration (sulfide in both dissolved form and bound in minerals). In this model,
189 Fe(II) is available at concentrations in equilibrium with siderite (as per Holland, 1984),
190 pH is determined by equilibrium with siderite and calcite at pCO_2 = 10X PAL (present
191 atmospheric level). We consider a pCO_2 of 10 times PAL as an intermediate value
192 between high-end estimates for pre-1.8 Ga (>100 PAL, Ohmoto et al., 2004) and the
193 modern. Total zinc is fixed at an approximately modern value of 10^{-8} M (consistent with
194 Zn concentrations derived from the IF record presented below, as well as those used by
195 Saito et al., 2003), and the system is effectively titrated with increasing quantities of
196 sulfide (total S-II added).

197 Our dataset of Zn in authigenic iron oxides includes new analyses and a
198 comprehensive literature compilation (SI Table 2). We assign iron formations to one of
199 four broad categories – Algoma IF, Superior IF, ironstones, and Phanerozoic
200 hydrothermal deposits. Algoma IF are characterized by limited areal extent and close
201 association with submarine volcanic sources. Superior IF are laterally extensive and
202 typically formed on continental shelves. Ironstones encompass Precambrian granular and
203 oolitic iron formations, as well as more modern iron oolite-pisolite occurrences that
204 formed in shallow, nearshore environments. Phanerozoic hydrothermal deposits represent
205 modern, oxic seawater deposits where Fe(III) deposition occurred near hydrothermal
206 sources (Bekker et al., 2010).

207 Zn was analyzed in drill core and fresh hand samples (i.e., samples collected in
208 the field from outcrop), which were sub-sampled, then powdered and subjected to trace
209 element analysis. Importantly, samples showing evidence of weathering, alteration or
210 signs of severe metamorphic or diagenetic overprinting were excluded. Exclusion criteria

include association with a lateritic profile, Fe concentrations greater than 60%, extensive veining, for all but Eoarchean samples recrystallization of chert to macrocrystalline quartz, intense folding, and above-greenschist facies metamorphism. Analyses were performed on powder digests or by *in situ* laser ablation (New Wave Research UP-213) using a Perkin Elmer Elan6000 Quadrupole – Inductively Coupled Plasma Mass Spectrometer (Q-ICP-MS) at the University of Alberta (U of A). Precision was monitored by repeated analyses of well-constrained international standards (BE-N Basalt, CRPG Nancy for digests and NIST SRM 610 or 612 for laser ablation). Sample analyses at Woods Hole Oceanographic Institute (WHOI) were conducted on a ThermoElectron Inc. Element 2 high-resolution sector field ICP-MS and precision and accuracy assessed by analysis of USGS geostandard BHVO-1. Sample selection and analytical methods are identical to our previous work (Konhauser et al., 2009, 2011) and are described in detail therein. At the U of A repeated analyses (n = 3) of BE-N produced a value for Zn of 128±19 ppm at the two standard deviation level, compared to a recommended value of 120±13 ppm. Repeat analyses of laser ablation standards NIST SRM 610 and 612 at the U of A yielded average values of 474±66 ppm (n = 46) and 38.7±5.0 ppm (n=31) at the single standard deviation level. These are compared to mean literature values for laser ablation of NIST STM 610 and 612 of 469±34 ppm and 40±2 ppm, respectively (Jochum et al., 2011). At WHOI repeated analysis of BHVO-1 produced a value for Zn of 91±19 ppm at the two standard deviation level, compared to a recommended value of 105±5ppm.

From a database of over 3800 new and literature IF analyses, 1660 have available Zn data, and of those, 590 samples passed filters for detrital contamination (<1% Al_2O_3

and <0.1% TiO_2; Fig. 2) and compatible mineralogy; the unfiltered and filtered records are presented in Fig 3A and B, respectively. Compatible mineralogies were restricted to Fe and Si-rich chemical sediments, thereby excluding volcanics, sulfides, and carbonates. For authigenic iron oxide sediments with low detrital contamination, molar Zn and Fe data were compared to hypothetical partitioning scenarios to constrain potential paleomarine Zn concentrations.

The simple partitioning models presented herein (lines in Figure 4) constitute an effort towards developing trace element proxies in IF that are better informed by the rock record itself and are independent of experimentally-determined partition coefficients. The slope in Zn-Fe space (a Zn/Fe ratio) is calculated by assuming quantitative precipitation of both Zn and Fe from a given volume of seawater, such that hypothetical seawater Zn and Fe concentration scenarios may be compared directly with rock record data. In reality, only a fraction of total dissolved Zn will be removed at any given time, but as this is also the case with Fe, and as Zn adsorption depends on available Fe(III) oxyhydroxide surface sites, partial co-removal of Zn and Fe approaches the scenario of quantitative removal proposed by the simple, hypothetical partitioning scenarios.

The hypothetical partitioning scenarios presented in Figure 4 are dependent on several important assumptions: (1) that adsorption occurred to Fe(III) oxyhydroxides, such that any particular trace element should scale with Fe (but not Si), (2) that maximum dissolved Fe concentrations may be constrained (as per Holland, 1984) by either mineral solubility (e.g., ~1-10 ppm for siderite) or sedimentation rate (e.g., 20 mg/cm^2 per year under a water column of at least 100 m, thus 2 ppm), and (3) that Zn and Fe precipitated quantitatively. Assumption (1) is supported by Fig. 4, and while assumption (3) is

257 unlikely, it is conservative in that a maximum estimate of partitioning efficiency and thus
258 a minimal potential seawater concentration is achieved.
259
260
261 **Results**
262 Results of the geochemical models are presented in Figure 1 and described in detail
263 herein. Mineral saturation indices (upper dashed lines) indicate that saturation with
264 respect to sphalerite is achieved at total sulfide concentrations over 10^{-9} M and limits total
265 dissolved Zn (combination of Zn^{2+} and ZnS) thereafter. Total sulfide concentrations
266 above 5 x 10^{-5} M (saturation with respect to mackinawite) are effectively excluded by the
267 S-poor mineralogy of IF samples. Three models are considered: (1) in the absence of
268 organic ligands (Fig. 1A), (2) with 1 nM of an uncharacterized organic ligand binding
269 Zn^{2+} with a conditional log K of 11, as described for Central North Pacific seawater by
270 Bruland (1989)(Fig. 1B), and (3) with 100 nM of the same organic ligand, as a sensitivity
271 test for historical differences in the availability of organic ligands (Fig. 1C). In all
272 models, total Zn concentration is effectively limited by the sulfide-dependent solubility of
273 sphalerite. In the absence of organic complexation (Fig. 1A), it can be seen that the
274 hydrated metal aquo complexes of Zn^{2+} and Fe^{2+} dominate under all conditions, with the
275 exception of the highest permitted sulfide concentrations, where Zn^{2+} and $ZnS_{(aq)}$ become
276 approximately equimolar (see discussion). When organic complexation of zinc is
277 considered, at modern concentrations of strong Zn binding ligands (~1-3 nM, Bruland,
278 1989; Jakuba et al., 2012), organic zinc complexes quickly become the dominant form of
279 dissolved Zn. When total S(-II) is further increased, sphalerite precipitation draws down

the total dissolved reservoir to parity with the strong Zn binding organic ligand (at ~10^{-7} M total S(-II) added). In the case of Zn-binding organic ligand concentrations 100X that of modern (Fig. 1C), regardless of the ambient sulfide concentration, the total dissolved Zn pool is effectively dominated by organic complexes, free Zn^{2+} is suppressed even under sulfide-poor regimes, and the total Zn inventory is buffered against sphalerite precipitation losses. While these geochemical models reaffirm a strong role for organic complexation in determining the bioavailable Zn pool, bioavailable Zn^{2+} does not descend significantly below concentrations considered limiting for all organisms investigated (10^{-12} M), unless upper water column depletion of Zn is also considered (see discussion).

Compositional data for modern and ancient authigenic iron oxides are presented in Figures 2 through 4. Zn concentrations in detritally-filtered samples average 130 ppm (nearly twice the upper crustal value of 67 ppm; Rudnick and Gao, 2003), with average molar Zn/Fe ratios of 0.00228 and a standard deviation of 0.0238. For samples with Al or Ti values above detrital filter cutoffs, Zn concentrations tend towards upper crustal values, suggesting an increased Zn contribution from siliciclastic sources (Fig. 2); samples below detrital filter cutoffs lack correlation of Zn with Al and Ti but show Zn concentrations that scale with Fe (Fig. 4). This indicates authigenic Zn enrichment conforming to distribution coefficient behavior in these samples. It is likely that Zn was acquired during initial ferric oxyhydroxide precipitation by adsorption processes (e.g., Benjamin and Leckie, 1981; Planavsky et al., 2010), which during the Archean and early Proterozoic, most likely occurred in the marine photic zone (Konhauser et al., 2002; Kappler et al., 2005; Planavsky et al., 2010).

Figure 3A-B display all available data and those passing detrital filters, respectively, as a time series of molar Zn/Fe ratios. While significant variability exists at any given time, the overall trend is a relatively static range in Zn/Fe over geological time, except for the most modern samples (see discussion). Figure 4A puts these ratios in perspective by presenting simple models for quantitative Zn removal at marine Fe concentrations of 179 μM (10 ppm) and near-modern Zn concentrations of 10 nM (0.65 ppb); nearly all data fall within the range predicted by our models and crucially, indicate paleomarine Zn concentrations within an order of magnitude of modern oceans. An iron concentration of 179 μM was applied as it represents the upper limit of conservative estimates based on the work of Holland (1984) and would subsequently correspond to the lowest estimate of paleomarine Zn (i.e., decreasing Fe from 179 to 17.9 μM results in increasing estimates for paleomarine Zn).

At assumed Fe concentrations of 179 μM, a minimum Zn concentration of 0.1 nM is indicated by Zn/Fe ratios preserved in ancient iron oxides, yet the majority of samples are well represented by a concentration within 10-fold of modern Zn values (Fig. 4A). Estimates are considered conservative as our models assume 100% adsorption of Zn onto the primary ferric oxyhydroxide; this quantitative scavenging relationship represents maximum possible partitioning efficiency and thereby returns a minimum possible concentration; partial Zn adsorption would lead to increased estimates for paleomarine Zn concentrations. Conversely, increased dissolved Fe concentrations would result in a decreased estimate of paleomarine Zn concentrations. However, even at a high-end estimate of 1790 μM Fe, realistic only for essentially undiluted hydrothermal fluids (Edmond et al., 1982) and ~30X higher than limits imposed by siderite solubility

(Holland, 1984), near modern Zn levels are still indicated by the authigenic iron mineral record (Fig. 4B). There exists a high level of agreement between the filtered and unfiltered records in this regard (Fig. 3; SI Fig. 1).

Discussion

Zn/Fe ratios in IF through time appear relatively constant (Fig. 3) despite dramatic changes in ocean chemistry from the Archean to today. The spread in Zn enrichments may be related to (1) vertical/lateral paleomarine spatial variability, (2) local or short-term fluctuations in the marine Zn reservoir, or (3) diagenetic effects. Firstly, it is anticipated that vertical/lateral spatial variability might be similar to that of modern oceans where Zn concentrations are heterogeneous between, and within, ocean basins. In terms of vertical distribution in the Precambrian, we expect that similar to today, enriched Zn fluids would resupply a depleted photic zone via diffusion and advection from deep waters. Future work examining Zn isotope compositions may reveal whether ancient upper water columns were depleted due to biological activity (c.f. Kunzmann et al., 2013). As the precipitation of metastable IF precursor minerals (e.g., ferrihydrite) likely occurred in the photic zone (e.g. Konhauser et al., 2002; Kappler et al., 2005), it is possible that the spread in IF values record dynamics in depletion of the upper water column. Secondly, it is a possibility that variation within a single basin (and thus IF deposit) may be driven by potential pulse-like influxes of Zn along with Fe resulting from episodic hydrothermal activity as well as a potential drawdown of Zn due to protracted IF deposition. Events such as these may account for the highest and lowest Zn/Fe ratios, respectively. Thirdly, little information is available regarding further Zn adsorption or

349 release upon iron mineral diagenesis or metamorphism. Experimental data indicates that
350 for Zn-ferrihydrite co-precipitates, aging and mineral transformation, with or without
351 added organics, has little effect on equilibrium Zn solubility (Martinez and McBride,
352 1999). With regards to metamorphism, Bhattacharya et al. (2007) presented a suite of IF
353 data from the Jharkhand-Orissa region, that showed similar Zn concentrations between
354 hydrothermally metasomatized IF and 'unaltered' IF in the same region. In addition,
355 samples used in our analyses were devoid of obvious supergene alteration (i.e., severe
356 chert re-crystallization, martite formation). These results, combined with the relatively
357 coherent rock record dataset provided here, suggest minimal post-depositional Zn
358 mobilization in IF. Given the comprehensive nature of our dataset, there are likely to be
359 some samples that have been affected by secondary mineralization. Mineralization,
360 however, is very unlikely to explain the overall trend of Zn abundances, a trend that
361 differs from other elements that are commonly enriched during secondary mineralization
362 (e.g. Cu, U) (Davidson and Large, 1994; Verma et al., 2003; Tallarico et al., 2005).
363 In addition to the three factors described above, variability in the IF record may
364 reflect subtle changes in the reactivity of the solid-phase iron minerals for dissolved Zn.
365 When considering only Precambrian data, linear regression between Zn and Fe is poorly
366 supported (SI Figure 1B); this may reflect variable contribution of less reactive and Zn-
367 poor reduced iron minerals such as siderite or greenalite, which would also introduce
368 variability in Zn/Fe ratios for any given deposit. Regression between Zn and Fe for
369 Phanerozoic samples is more robust, and along similar lines might reflect a fully oxidized
370 and thus consistently zinc-reactive aspect of Phanerozoic hydrothermal iron precipitates.
371 Indeed, a 10-100 fold increase in the Zn/Fe ratio of recent sediments may reflect the

372 rapidity of Fe(III) precipitation under a fully oxygenated water column, resulting in
373 increased contribution of Zn from enriched hydrothermal fluids proximal to modern
374 vents. Under oxic conditions, iron mineral precipitation in closer proximity to
375 hydrothermal sources, as well as a lack of co-precipitating reduced and thus Zn-poor iron
376 mineral phases, could explain both the tighter relationship between Zn and Fe and the
377 recent rise in Zn/Fe observed for the Phanerozoic.

378 In pyritic marine sediments, there is an apparent relationship between the degree
379 to which a metal is preferentially hosted in pyrite (degree of trace metal pyritization,
380 DTMP) and log $K_{metal\text{-}S}/K_{FeS}$ (see Morse and Luther, 1999; their Figure 3). This feature is
381 akin to a linear free-energy relationship between the equilibrium partitioning of trace
382 metals into pyrite and the equilibrium solubility of individual trace metal sulfide mineral
383 phases, and is characteristic of trace metal substitution into pyrite (Morse and Luther,
384 1999). Zn, as well as Cd and Pb, depart significantly from this trend in that they are
385 anonymously low in concentration in the pyrite fraction of pyritic marine sediments,
386 indicating that these elements are primarily sequestered as independent mineral phases
387 rather than as a minor constituent of pyrite, likely as a natural consequence of the faster
388 kinetics of their precipitation as metal sulfides (Morse and Luther, 1999). Accordingly,
389 sphalerite (ZnS) solubility imposes an upper boundary on dissolved Zn in the presence of
390 sulfide (e.g., Hsu-Kim et al., 2008). The formation of strong Zn-S complexes may further
391 act to limit free Zn^{2+} under euxinic conditions (e.g., Landing & Lewis, 1992).
392 Geochemical modeling (Fig. 1) demonstrates that under the ferruginous conditions
393 necessary for the deposition of Precambrian IF, aqueous complexation and drawdown of
394 bioavailable Zn^{2+} by sulfide may not be as important as previously thought. Saito et al.

(2003) performed similar speciation calculations for Co, Fe, Mn, Zn, Ni, Cu, and Cd under hypothetical 'ferro-sulfidic' Archean ocean conditions, and indicated that the vast majority (>99%) of dissolved Zn should be complexed with sulfide as $ZnS_{(aq)}$. However, upon re-examination of Zn speciation for this study, it appears the conditional stability constant of the $ZnS_{(aq)}$ species was not parameterized correctly in Saito et al. (2003), leading to an overestimation of this species' abundance, while the other metal species were correctly parameterized. In our current modeling effort, such high degrees of aqueous Zn complexation by sulfide do not occur until well after supersaturation with respect to mackinawite (FeS) is reached (Fig. 1). Such high sulfide concentrations are effectively excluded by the fact that, with the exception of some highly reduced Algoma-type iron formations, iron sulfide minerals are typically absent. A lack of correlation between Zn and S in our dataset (see SI Fig. 2) further suggests a minimal role for S in Zn sequestration under Fe(III) oxyhydroxide depositional conditions. Several limitations also exist with respect to the thermodynamic modeling of ZnS complexes. For instance, modeling is dependent on the stoichiometry of modeled ZnS complexes and their respective stability constants; Rickard and Luther (2006) provide a short summary of ZnS complexation and list eleven possible ZnS complexes, several for which stability constants vary depending on the method used for determination.

In ancient oceans heterogeneous with respect to sulfide content (e.g., Poulton et al., 2010; Planavsky et al., 2011) and where sulfide effectively titrates iron such that the siderite-buffering effect inherent to our models no longer occurs, it is possible that bioavailable Zn would have been drawn down below biolimiting concentrations in sulfide-rich zones as per Saito et al. (2003). However, these zones were likely restricted

418 to near shore and other high productivity regions of the oceans (e.g., Poulton et al., 2010).
419 In such instances, Zn may have been buffered against sulfide by organic ligand
420 complexation (Fig 1B and C), potentially becoming bioavailable again once reaching the
421 overlying oxic or underlying ferruginous waters. It seems unlikely given the consistency
422 of the shales and IF record (Scott et al., 2013; this work), that sulfide water masses
423 controlled Zn bioavailability throughout much of the Precambrian. Accordingly, the Zn
424 speciation model presented here for IF depositional conditions implies that bioavailable
425 (non-complexed) Zn may well have been abundant and readily available to primitive
426 eukaryotes.

427 An important alternative to the modeling described thus far is the possibility that
428 strong and persistent organic complexes of zinc may have played an important role in
429 controlling Zn solubility, speciation and possibly bioavailability. This scenario is
430 modeled in Figures 1B and 1C, and demonstrates that organic complexation of Zn plays a
431 crucial role in determining the speciation of the reservoir, such that whenever the
432 concentrations of strong Zn-binding organic ligands approach that of total dissolved Zn,
433 organic Zn complexes will dominate the dissolved pool. Considering that poorly-
434 ventilated and reducing ocean conditions would have acted to stabilize strong organic
435 ligands in seawater, such as those with reduced sulfur groups (e.g., thiols and cysteine-
436 rich peptides), the possibility that organic complexation of Zn played a more important
437 role in the Precambrian cannot be excluded. It, therefore, represents a strong caveat to the
438 interpretations presented herein, potentially limiting the bioavailability of Zn.
439 Interestingly in the modern ocean, strong Zn-complexing ligands appear only in the upper
440 water column (Bruland, 1989; Jakuba et al., 2012) where they are likely continually

441 produced by microbial phytoplankton (Lohan et al., 2002). By contrast, in the deeper
442 oxygenated water column, these ligands are subsequently oxidized, and the sorbed Zn is
443 released back into solution. How this potential scenario would have influenced the
444 evolution of nutritional requirements is not clear; there is recent data indicating that the
445 complexation of Zn by organic ligands can actually enhance phytoplankton Zn uptake
446 (Aristilde et al., 2012). Such high affinity systems may have come at a metabolic cost, but
447 could also have allowed access to this useful structural metal cation. It should be
448 emphasized that the bioavailability of Zn-organic ligand complexes has a strong bearing
449 on the interpretation of the second scenario. If Zn bound by organic ligands was indeed
450 bioavailable in the Precambrian, it would suggest that under any of the conditions
451 postulated here, Zn would be bioavailable to early eukaryotes. This would effectively
452 represent a case where the two proposed scenarios become complimentary.

453 The two chemical speciation scenarios presented here, both constrain the
454 bioavailable Zn inventory and have significant implications for paleomarine Zn
455 geochemistry. In the first scenario where Zn speciation was not dominated by organic
456 complexes, periods of ocean euxinia would have caused significant depletion of the
457 oceanic Zn inventory due to precipitation of sphalerite with increased oceanic sulfide
458 abundances (Fig. 1A). Such events may not have been captured by the IF record
459 presented here due to the chemical incompatibility of extensive euxinia and the
460 deposition of IF, but should be observable in parallel shale records (Scott et al., 2013).
461 Periods of expanded euxinia could have conceivably caused considerable oceanic Zn
462 inventory instability, which itself could have been a temporal selection pressure against
463 early adoption of Zn ions in metalloenzymes. However, relatively stable sedimentary

concentrations indicated by both the IF (this work) and shale records (Scott et al., 2013) may be envisioned as a result of the second scenario, where oceanic Zn speciation is dominated by organic complexes such that the total Zn inventory would have remained stabilized despite large scale variations in the extent of euxinic marine conditions (Fig. 1C). Direct measurement of low-level Zn speciation conditions in analogous modern environments may contribute to our understanding of which of these scenarios may have dominated. Moreover, future modeling work is planned to better understand the factors controlling the aqueous complexation of zinc by sulfide and organic ligands, and their sensitivity to model presuppositions under ferruginous and euxinic ancient ocean chemistry scenarios.

The persistence of a zinc inventory on the order of magnitude of modern oceans throughout history is particularly curious given the late expansion of Zn-binding domains in eukaryotes (Dupont et al., 2006; 2010). It is possible that the relatively late expansion of Zn-binding proteins over the course of eukaryotic metallome evolution reflected the regulatory needs inherent to increasingly complex genomes (see also Scott et al., 2013). Late-evolving Zn-binding domains in eukaryotic genomes are predominately structural and localized to the nucleus, specifically in DNA regulating elements (Dupont et al., 2010). Power-law scaling of Zn-binding domains as a function of total proteome size is >1 for *Eukarya* but <1 for *Archaea* and *Bacteria* (c.f. Fig S1 from Dupont et al., 2010). Essentially, eukaryotic genomes possess greater numbers of Zn-binding proteins with increasing genome size while prokaryotic genomes follow the opposite trend, suggesting that the difference in metallome composition may reflect the dramatic differences in eukaryotic and prokaryotic genome regulation. The proliferation of structural, nucleus-

bound Zn-binding domains should be expected to accompany rapid evolutionary innovation during late Proterozoic eukaryote diversification in body plans. Future phylogenetic work examining the expansion of eukaryotic Zn-binding domains in light of their specific roles in eukaryotic homeostasis may be able to confirm or deny such a hypothesis. Despite uncertainties relating to organic complexation of Zn in ancient oceans, this work provides important constraints and insight into the evolution of the Zn metallome, and the possibilities regarding intrinsic and biological influences, versus extrinsic and geochemical, driving forces.

Conclusion

We conclude that the record of Zn enrichments in IF points toward a relatively constant marine Zn reservoir through geological time, with paleomarine concentrations within an order of a magnitude of modern values throughout much of the Precambrian. Equilibrium speciation modeling reveals that under IF depositional conditions and modern organic ligand concentrations, the Zn reservoir should have been dominated by free and bioavailable Zn^{2+}, with aqueous Zn complexation by sulfide becoming important (>50% of the total dissolved reservoir) only at sulfide concentrations reaching FeS mineral saturation. Our finding of a near modern bioavailable Zn reservoir through time as recorded by the IF record, and supported by detailed geochemical models, is also in line with that of the other common sedimentary proxy for paleomarine conditions, the euxinic shale record (Scott et al., 2013). The agreement between these records testifies to the robustness of the model presented here. Furthermore, strong organic complexes of Zn, for example involving structures with reduced sulfur groups of high Zn affinity, may have

been more important in ancient oceans for lack of an oxidative sink. This may have allowed stabilization of the Zn inventory through both ferruginous and euxinic ocean conditions, but potentially may have depressed Zn bioavailability, as the availability of Zn-organic complexation is not fully understood.

Together, this IF-based inventory and chemical speciation study places constraints on our understanding of the geochemical evolution of the Precambrian Zn reservoir and its potential coupling to eukaryotic metallome evolution. A novel possibility stemming from this work is that the late proliferation of Zn metalloenzymes in eukaryotes could have been a biologically intrinsic process related to the regulation of increasingly complex genomes, rather than solely dependent on the dramatic changes in the marine bioavailability of aqueous Zn species.

Acknowledgements

We thank Guangcheng Chen for his assistance with laser ICP-MS and bulk digest analyses. We also thank the three anonymous reviewers for their insightful comments that have greatly improved this manuscript. This work was supported by a NSERC Discovery Grant to KOK, a NSERC PDF to SVL, a NSERC CGSM to LJR, and an NSF-EAR-PDF to NJP. MAS acknowledges support from the Gordon and Betty Moore Foundation Grant #2724. This work was also supported by grants from the Deutsche Forschungsgemeinschaft (DFG) to A.K. (KA 1736/4-1 and 12-1).

References

1. Anbar AD, Knoll AH (2002) Proterozoic ocean chemistry and evolution: A bioinorganic bridge? *Science*, **297**, 1137-1142.
2. Aristilde L, Xu Y, Morel FMM (2012) Weak organic ligands enhance zinc uptake in marine phytoplankton. *Environmental Science and Technology*, **46**, 5438-5445.
3. Bhattacharya HN, Chakraborty I, Ghosh KK (2007) Geochemistry of some banded iron-formations of the archean supracrustals, Jharkhand-Orissa region, India. *Journal of Earth System Science*, **116**, 245-259.
4. Bekker A, Slack JF, Planavsky N, Krapež B, Hofmann A, Konhauser KO, Rouxel OJ (2010) Iron Formation: The sedimentary product of a complex interplay among mantle, tectonic, oceanic and biospheric processes. *Economic Geology*, **105**, 468-508.
5. Benjamin MM, Leckie JO (1981), Multiple-site adsorption of Cd, Cu, Zn, and Pb on amorphous iron oxyhydroxide. *Journal of Colloid and Interface Science*, **79**, 209-221.
6. Berg JM, Shi Y (1996) The galvanization of biology: a growing appreciation for the roles of zinc. *Science*, **271**, 1081-1085.
7. Brand LE, Sunda WG, Guillard RRL (1983) Limitation of marine phytoplankton reproductive rates by Zinc, Manganese, and Iron. *Limnology and Oceanography*, **28**, 1182-1198.
8. Bruland KW (1980) Oceanographic distributions of cadmium, zinc, nickel, and copper in the north pacific. *Earth and Planetary Science Letters*, **47**, 176-198.
9. Bruland KW (1989) Complexation of Zinc by natural organic ligands in the Central North Pacific. *Limnology and Oceanography*, **34**, 269-285.

555 10. Bruland KW, Orians KJ, Cowen JP (1994) Reactive trace metals in the stratified
556 central North Pacific. *Geochimica et Cosmochimica Acta*, **58**, 3171-3182.
557 11. Crawford DW, Lipsen MS, Purdie DA, Lohan MC, Statham PJ, Whitney FA, Putland
558 JN, Johnson WK, Sutherland N, Peterson TD, Harrison PJ, Wong CS (2003)
559 Influence of zinc and iron enrichments on phytoplankton growth in the Northeastern
560 Subarctic Pacific. *Limnology and Oceanography*, **48**, 1583-1600.
561 12. Coale KH, Michael Gordon R, Wang X (2005) The distribution and behavior of
562 dissolved and particulate iron and zinc in the Ross Sea and Antarctic circumpolar
563 current along 170ºW. *Deep Sea Research I*, **52**, 295-318.
564 13. Davidson GJ, Large RR (1994) Gold metallogeny and the copper-gold association of
565 the Australian Proterozoic. *Mineralium Deposita* **29**, 208-223.
566 14. Doe BR (1994) Zinc, copper, and lead in mid-ocean ridge basalts, and the source rock
567 control on Zn/Pb in ocean-ridge hydrothermal deposits. *Geochimica et Cosmochimica*
568 *Acta*, **58**, 2215-2223.
569 15. Duce RA, Liss PS, Merrill JT, Atlas, EL, Buat-Menard P, Hicks BB, Miller MJ,
570 Prospero JM, Arimoto R, Church TM, Ellis W, Galloway JN, Hansen L, Jickells TD,
571 Knap AH, Reinhardt KH, Schneider B, Soudine A, Tokos JJ, Tsunogai S, Wollast R,
572 Zhou M (1991) The atmospheric input of trace species to the world ocean. *Global*
573 *Biogeochemical Cycles*, **5**, 193-259.
574 16. Dupont CL, Yang S, Palenik B, Bourne PE (2006) Modern proteomes contain
575 putative imprints of ancient shifts in trace metal geochemistry. *Proceeding of the*
576 *National Academy of Sciences*, **103**, 17822-17827.

17. Dupont CL, Butcher A, Valas RE, Bourne PE, Caetano-Anollés G (2010) History of biological metal utilization inferred through phylogenetic analysis of protein structures. *Proceedings of the National Academy of Sciences*, **107**, 10567-10572, doi: 10.1073/pnas.0912491107.

18. Edgcomb VP, Molyneaux SJ, Saito MA, Lloyd K, Böer S, Wilson CO, Atkins MS, Teske A (2004) Amelioration of metal toxicity by sulphide for Archaea at deep-sea hydrothermal vents. *Applied Environmental Microbiology*, **70**, 2551-2555.

19. Edmond JM, Von Damm KL, McDuff RE, Measures CI, (1982) Chemistry of hot springs on the East Pacific Rise and their effluent dispersal. *Nature*. **297**, 187-191.

20. Franck VM, Bruland KW, Hutchins DA, Brzezinski MA (2003) Iron and zinc effects on silicic acid and nitrate uptake kinetics in three high-nutrient, low-chlorophyll (HNLC) regions. *Marine Ecology Progress Series*, **252**, 15-33.

21. Gardner LR (1974) Organic versus inorganic trace metal complexes in sulfidic marine waters – some speculative calculations based on available stability constants. *Geochimica et Cosmochimica Acta*, **38**, 1297-1302.

22. German CR, Campbell AC, Edmond JM (1991) Hydrothermal scavenging at the Mid-Atlantic Ridge: modification of trace element dissolved fluxes. *Earth and Planetary Science Letters*, **107**, 101-114.

23. Gustafsson JP (verified 10 October 2012). Visual Minteq 3.0: http://www2.lwr.kth.se/English/OurSoftware/vminteq.

24. Holland HD (1984) *The Chemical Evolution of the Atmosphere and Oceans*. Princeton University Press, New Jersey.

25. Hsu-Kim H, Mullaugh KM, Tsang JJ, Ucel M, Luther GW III (2008) Formation of Zn- and Fe-sulfides near hydrothermal vents at the Eastern Lau Spreading Center: implications for sulfide bioavailability to chemoautotrophs. *Geochemical Transactions*, **9**:6.

26. Jakuba RW, Saito MA, Moffett JW, Bidigare B, Xu Y (2012) Dissolved zinc in the North Pacific: Distribution, speciation, and importance to primary producers. *Global Biogeochemical Cycles,* **26**, GB2015.

27. Jochum KP, Weis U, Stoll B, Kuzmin D, Yang Q, Raczek I, Jacob DE, Stracke A, Birbaum K, Frick DA, Günther D, Enzweiler J (2011) Determination of reference values for NIST SRM 610-617 glasses following ISO guidelines. *Geostandards and Geoanalytical Research*, **35**, 397-429.

28. John SG (2007) The marine biogeochemistry of zinc isotopes. PhD thesis, MIT/WHOI, Cambridge, Massachusetts, 2007-2008.

29. Klein C (2005) Some Precambrian banded iron-formations (BIFs) from around the world: Their age, geological setting, mineralogy, metamorphism, geochemistry and origin. *American Mineralogist*, **90**, 1473-1499.

30. Kappler A, Pasquero C, Konhauser KO, Newman DK (2005) Deposition of banded iron formations by anoxygenic phototrophic Fe(II)-oxidizing bacteria. *Geology*, **33**, 865-868.

31. Konhauser KO, Hamade T, Raiswell R, Morris RC, Ferris FG, Southam G, Canfield DE (2002) Could bacteria have formed the Precambrian banded iron formation? *Geology*, **30**, 1079-1082.

32. Konhauser KO, Pecoits E, Lalonde SV, Papineau D, Nisbet EG, Barley ME, Arndt NT, Zahnle K, Kamber BS (2009) Oceanic nickel depletion and a methanogen famine before the Great Oxidation Event. *Nature*, **458**, 750-753.

33. Konhauser, KO Lalonde SV, Planavsky NJ, Pecoits E, Lyons TW, Mojzsis SJ, Rouxel OJ, Barley ME, Rosìere C, Fralick PW, Kump LR, Bekker A (2011) Aerobic bacterial pyrite oxidation and acid rock drainage during the Great Oxidation Event. *Nature*, **478**, 369-373.

34. Kunzmann M, Halverson GP, Sossi PA, Raub TD, Payne JL, Kirby J (2013) Zn isotope evidence for immediate resumption of primary productivity after snowball Earth. *Geology*, **41**, 27-30.

35. Landing WM, Burnett WC, Lyons WB, Orem WH (1991) Nutrient Cycling and the Biogeochemistry of Manganese, Iron, and Zinc in Jellyfish Lake, Palau. *Limnology and Oceanography*, **36**, 515-525.

36. Landing WM, Lewis BL (1992) Thermodynamic modeling of trace element speciation in the Black Sea. In: *Black Sea Oceanography* (eds. Izdar E, Murray JW). NATO-ASI Series C, **351,** Kluwer Academic Publishers, Netherlands, pp. 125-160.

37. Lohan MC, Statham PJ, Crawford DJ (2002) Total dissolved zinc in the upper water column of the subarctic North East Pacific. *Deep-Sea Research II: Topical Studies in Oceanography*, **49**, 5793-5808.

38. Luther GW, Rickard DT, Theberge S, Olroyd A (1996) Determination of metal (bi)sulfide stability constants of Mn^{2+}, Fe^{2+}, Co^{2+}, Ni^{2+}, Cu^{2+}, and Zn^{2+} by voltammetric methods. *Environmental Science & Technology*, **30**, 671-679.

39. Luther GW, Theberge SM, Rickard DT (1999) Evidence for aqueous clusters as

644 intermediates during zinc sulfide formation. *Geochimica et Cosmochimica Acta*, **63**,
645 3159-3169.
646 40. Maret W (2001) Zinc biochemistry, physiology, and homeostasis- recent insights and
647 current trends. *Biometals*, **14**, 187-190.
648 41. Martinez CE, McBride MB (1999) Dissolved and labile concentrations of Cd, Cu, Pb,
649 and Zn in aged ferrihydrite-organic matter systems. *Environmental Science and*
650 *Technology*, **33**, 745-750.
651 42. Morris RC (1993) Genetic modeling for banded iron-formation of the Hamersley
652 Group, Pilbara Craton, Western Australia. *Precambrian Research*, **60**, 243-286.
653 43. Morse JW and Luther GW III (1999) Chemical influences of trace metal-sulfide
654 interactions in anoxic sediments. *Geochimica et Cosmochimica Acta*, **63**, 3373-3378.
655 44. Nolting RF, de Baar HJW (1994) Behaviour of nickel, copper, zinc and cadmium in
656 the upper 300 m of a transect in the Southern Ocean (57º-62ºS, 49ºW). *Marine*
657 *Chemistry*, **45**, 225-242.

658 45. Ohmoto H, Watanabe Y, Kumazawa K (2004) Evidence from massive siderite beds
659 for a CO_2-rich atmosphere before ~1.8 billion years ago. *Nature*, **429**, 395-399.

660 46. Planavsky NJ, Bekker A, Rouxel OJ, Kamber B, Hofmann A, Knudsen A, Lyons TW
661 (2010) Rare Earth Element and yttrium compositions of Archean and
662 Paleoproterozoic Fe formations revisited: New perspectives on the significance and
663 mechanisms of deposition. *Geochimica et Cosmochimica Acta*, **74**, 6387-6405.

664 47. Planavsky NJ, McGoldrick P, Scott CT, Li C, Reinhard CT, Kelly AE, Chu X,
665 Bekker A, Love GD, Lyons TW (2011) Widespread iron-rich conditions in the mid-
666 Proterozoic ocean. *Nature*, **477**, 448-451.
667 48. Poulton SW, Fralick PW, and Canfield DE (2010) Spatial variability in oceanic redox
668 structure 1.8 billion years ago. *Nature Geoscience*, **3**, 486-490, doi:
669 10.1038/NGEO0889.
670 49. Rickard D, Luther III GW (2006) Metal sulfide complexes and clusters. *Reviews in*
671 *Mineralogy & Geochemistry*, **61**, 421-504.
672 50. Rudnick RL, Gao S (2003) Composition of the continental crust. In: Treatise on
673 Geochemistry, Volume 3 (eds. Holland HD, Turekian KK). Elsevier Science,
674 Amsterdam, Netherlands, p. 1-64.
675 51. Saito MA, Moffett JW, Chisholm SW, Waterbury JB (2002) Cobalt limitation and
676 uptake in *Prochlorococcus*. *Limnology and Oceanography*, **47**, 1629-1636.
677 52. Saito MA, Sigman DM, and Morel FMM (2003) The bioinorganic chemistry of the
678 ancient ocean: the co-evolution of cyanobacterial metal requirements and
679 biogeochemical cycles at the Archean-Proterozoic boundary? *Inorganica Chimica*
680 *Acta*, **356**, 308-318.
681 53. Scott C, Planavsky NJ, Dupont CL, Kendall B, Gill B, Robbins LJ, Husband KF,
682 Arnold GL, Wing B, Poulton SW, Bekker A, Anbar AD, Konhauser KO, Lyons TW
683 (2013) Bioavailability of zinc in marine systems through time. *Nature Geoscience*, **6**,
684 125-128.

54. Shaked Y, Xu Y, Leblanc K, Morel FMM (2006) Zinc availability and alkaline phosphatase activity in *Emiliania huxleyi*: Implications for Zn-P co-limitation in the ocean. *Limnology and Oceanography*, **51**, 299-309.

55. Sleep NH, Windley BF (1982) Archean Plate Tectonics: Constraints and Interferences. *The Journal of Geology*, **90**, 363-379.

56. Sunda W, Huntsman SA (1995) Cobalt and zinc interreplacement in marine phytoplankton: Biological and geochemical implications. *Limnology and Oceanography*, **40**, 1404-1417.

57. Tallarico FHB, Figueiredo BR, Groves DI, Kositcin N, McNaughton NJ, Fletcher IR, Rego JL (2005) Geology and SHRIMP U-PB Geochronology of the Igarapé Bahia Deposit, Carajás Copper-Gold Belt, Brazil: An Archean (2.57 Ga) Example of Iron-Oxide Cu-Au-(U-REE) Mineralization. *Economic Geology*, **100**, 7-28.

58. Tortell PD, Price NM (1996), Cadmium toxicity and zinc limitation in centric diatoms of the genus *Thalassiosira*. *Marine Ecology Progress Series*, **138**, 245-254.

59. Trocine RP, Trefy JH (1988) Distribution and chemistry of suspended particles from an active hydrothermal vent site on the Mid-Atlantic Ridge at 26ºN. *Earth and Planetary Science Letters*, **88**, 1-15.

60. Verma, MB, Roy MK, Saxena VP (2003) Uranium and Polymetallic Sulphide Mineralisation in the Banded Iron Formation at Udaisagar, Udaipur District, Rajasthan. *Journal of the Geological Society of India*, **61**, 703-710.

61. Wheat GC, Mottl MJ, Rudnick M (2002) Trace element and REE composition of a low-temperature ridge-flank hydrothermal spring. *Geochimica et Cosmochimica Acta*, **66**, 3693-3705.

62. Williams RJP, da Silva JJRF (1996) The Natural Selection of the Chemical Elements. Bath Press Ltd., Great Britain.

63. Zirino A, Yamamoto S (1972) A pH-dependent model for the chemical speciation of copper, zinc, cadmium and lead in seawater. *Limnology and Oceanography*, **17**, 661-671.

FIGURES

Figure 1. Modeled chemical equilibrium concentrations for major Zn and Fe species and mineral saturation indices (IAP/K_{sp}) as a function of total sulfide (HS^-) added for simulated seawater with (A) no organic complexation, (B) organic complexation as described for central north Pacific seawater (Bruland, 1989), and (C) same as (B) but with 100X higher organic ligand concentration. Blue lines represent inorganic Zn species, orange lines represent inorganic Fe species, green lines represent sulfide species, and red/burgundy lines represent organic ligands. Modeling was performed with visual MINTEQ 3.0 (Gustafsson, 2011) under anoxic conditions, at 25°C, 0.56 M NaCl and a pCO_2 of 10 times present atmospheric levels. Zn and Fe hydroxide and chloride species were also considered but are not plotted. The default thermodynamic database was adapted to account for multiple ZnS complexes and organic complexation (SI Table 1). Saturation with respect to calcite and siderite was assumed in all models and ultimately determined Ca and Fe concentrations, as well as pH, the latter ranging from 7.70 – 7.74 over the S(-II) range considered. Zn-S complexes included in SI Table 1, but not present in Figure 1, are not indicated to exist at significant levels. Mineral saturation indices equal to one indicates saturation; in this model supersaturation was not permitted, such that changes in total dissolved Zn and Fe are directly linked to mineral precipitation or dissolution. The grey area represents saturation with respect to Mackinawite and is excluded by the sulfide-deplete mineralogy of IF.

Figure 2. Cross-plots of Zn versus (A) Al_2O_3 and (B) TiO_2. Dashed lines represent detrital contamination cutoffs of 1 and 0.1 weight percent for Al_2O_3 and TiO_2,

739 respectively. Black lines correspond to crustal values for Zn (67 ppm (Rudnick and Gao,
740 2003)) and indicate that above these cutoffs, Zn in IF approach crustal values. Colors
741 correspond to varying IF types: Algoma (black), Superior (red), ironstone (blue) and
742 Phanerozoic hydrothermal (green); c.f. methods. Additionally, circles represent laser
743 ablation data and squares indicate analyses after bulk digestion.
744
745 **Figure 3** (A) Unfiltered record of available molar Zn/Fe data in authigenic iron oxides
746 through time, comprising Precambrian iron formation, Phanerozoic ironstones, and
747 exhalites. When samples with appreciable detrital or hydrothermal influence are included
748 in the record, there is a greater degree of variation than in the filtered record (B) Molar
749 Zn/Fe ratios in authigenic iron oxides, spanning Archean through Proterozoic IF,
750 Phanerozoic ironstones and exhalites; filtered for detrital contamination as per Figure 2.
751 Variability in Zn/Fe ratios at a given time may reflect heterogeneous marine Zn
752 distributions, temporal variations (e.g. Zn drawdown during protracted deposition), or
753 potential diagenetic modification. Importantly, no Zn/Fe data exists in our compilation
754 that suggests the low, biolimiting dissolved Zn concentrations previously predicted by
755 chemical equilibrium models for Precambrian oceans (Saito et al., 2003). Symbols as per
756 Fig. 2.
757
758 **Figure 4** (A) Zn-Fe cross plot revealing paleomarine Zn partitioning recorded by the
759 authigenic iron oxide record. Lines represent conservative models of Zn-Fe co-
760 precipitation behavior for hypothetical paleomarine Zn and Fe reservoirs, including those
761 previously predicted by chemical equilibrium modeling (Saito et al., 2003). Near-modern

762 paleomarine Zn concentrations are clearly indicated regardless of sample age. (B) Zn-Fe
763 cross plot further restricting paleomarine Zn concentrations under expanded boundaries
764 of hypothesized paleomarine Fe conditions. Even at elevated Fe concentrations of 1790
765 μM (100 ppm), a dissolved Zn concentration of ~1/10 of modern (1 nM) is indicated. At
766 low total Fe concentrations (1.79 μM), a dissolved Zn concentration of ~10 nM,
767 effectively that of modern oceans, is still indicated. Symbols as per previous figures.
768
769
770
771

a)

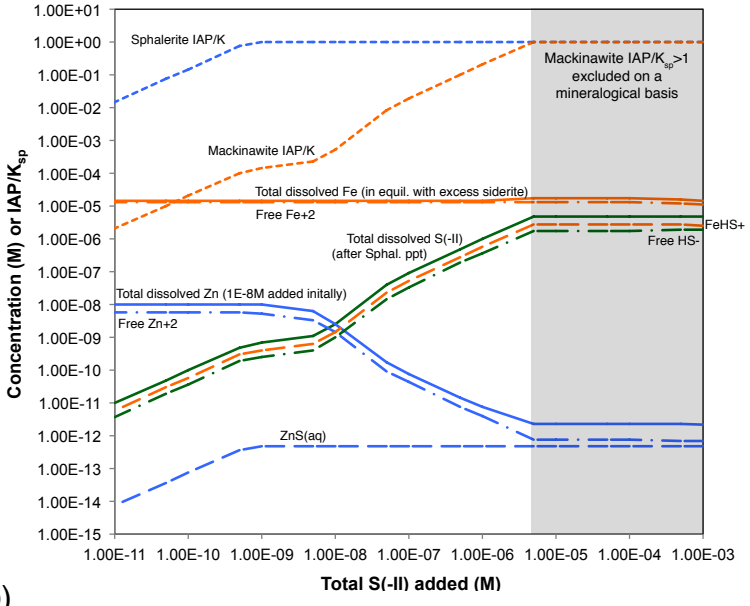
Sphalerite IAP/K
Mackinawite IAP/K
Mackinawite IAP/K$_{sp}$>1 excluded on a mineralogical basis
Total dissolved Fe (in equil. with excess siderite)
Free Fe+2
Total dissolved S(-II) (after Sphal. ppt)
FeHS+
Free HS-
Total dissolved Zn (1E-8M added initally)
Free Zn+2
ZnS(aq)
Concentration (M) or IAP/K$_{sp}$
Total S(-II) added (M)

b)

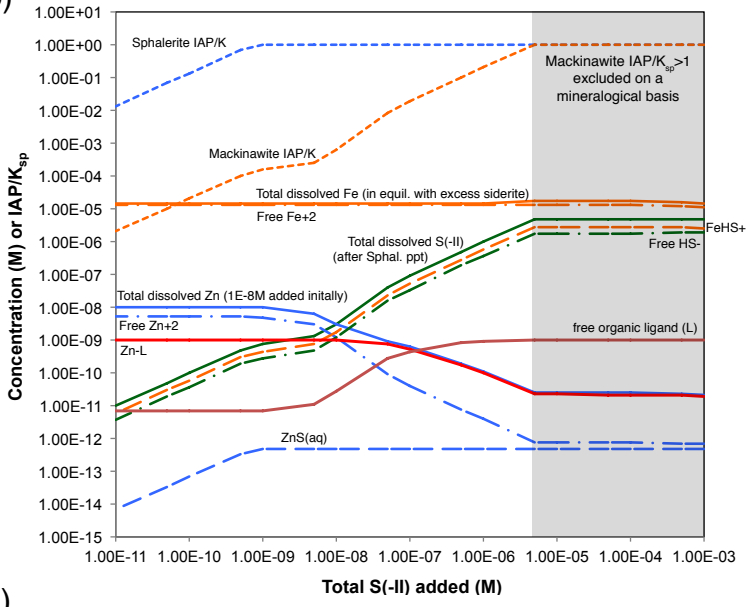
Sphalerite IAP/K
Mackinawite IAP/K
Mackinawite IAP/K$_{sp}$>1 excluded on a mineralogical basis
Total dissolved Fe (in equil. with excess siderite)
Free Fe+2
Total dissolved S(-II) (after Sphal. ppt)
FeHS+
Free HS-
Total dissolved Zn (1E-8M added initally)
Free Zn+2
Zn-L
free organic ligand (L)
ZnS(aq)
Concentration (M) or IAP/K$_{sp}$
Total S(-II) added (M)

c)

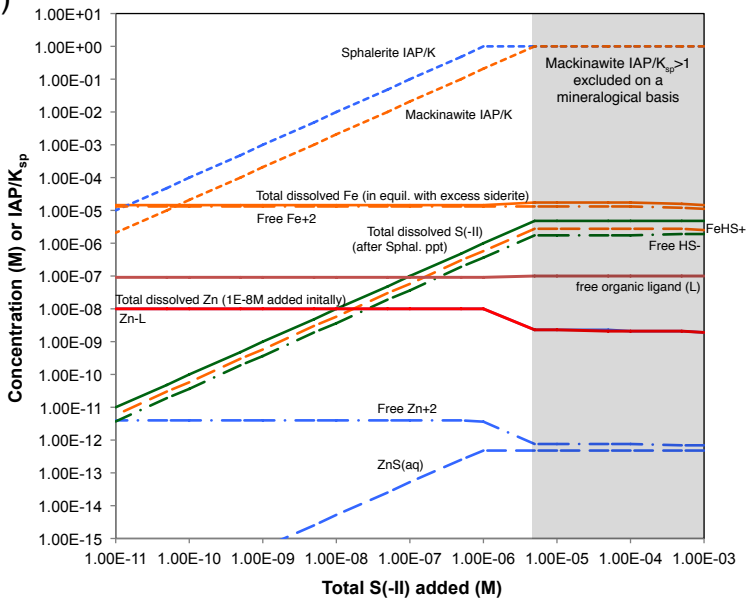
Sphalerite IAP/K
Mackinawite IAP/K
Mackinawite IAP/K$_{sp}$>1 excluded on a mineralogical basis
Total dissolved Fe (in equil. with excess siderite)
Free Fe+2
Total dissolved S(-II) (after Sphal. ppt)
FeHS+
Free HS-
free organic ligand (L)
Total dissolved Zn (1E-8M added initally)
Zn-L
Free Zn+2
ZnS(aq)
Concentration (M) or IAP/K$_{sp}$
Total S(-II) added (M)

a)

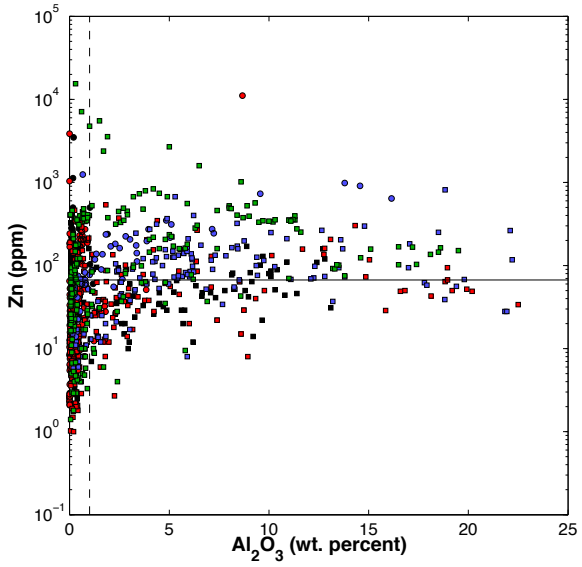

b)

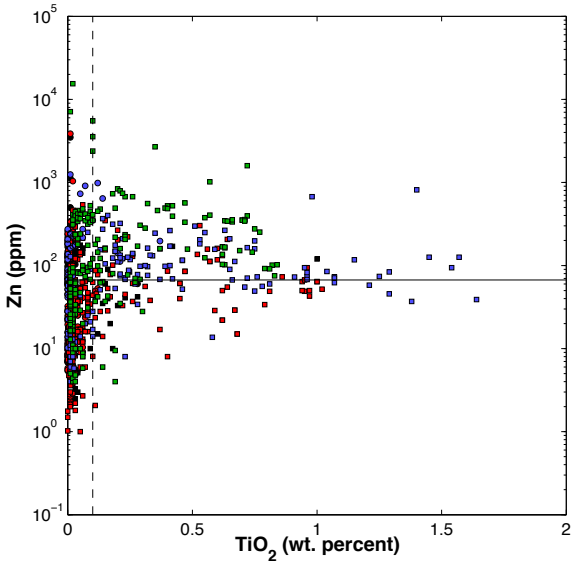

a)

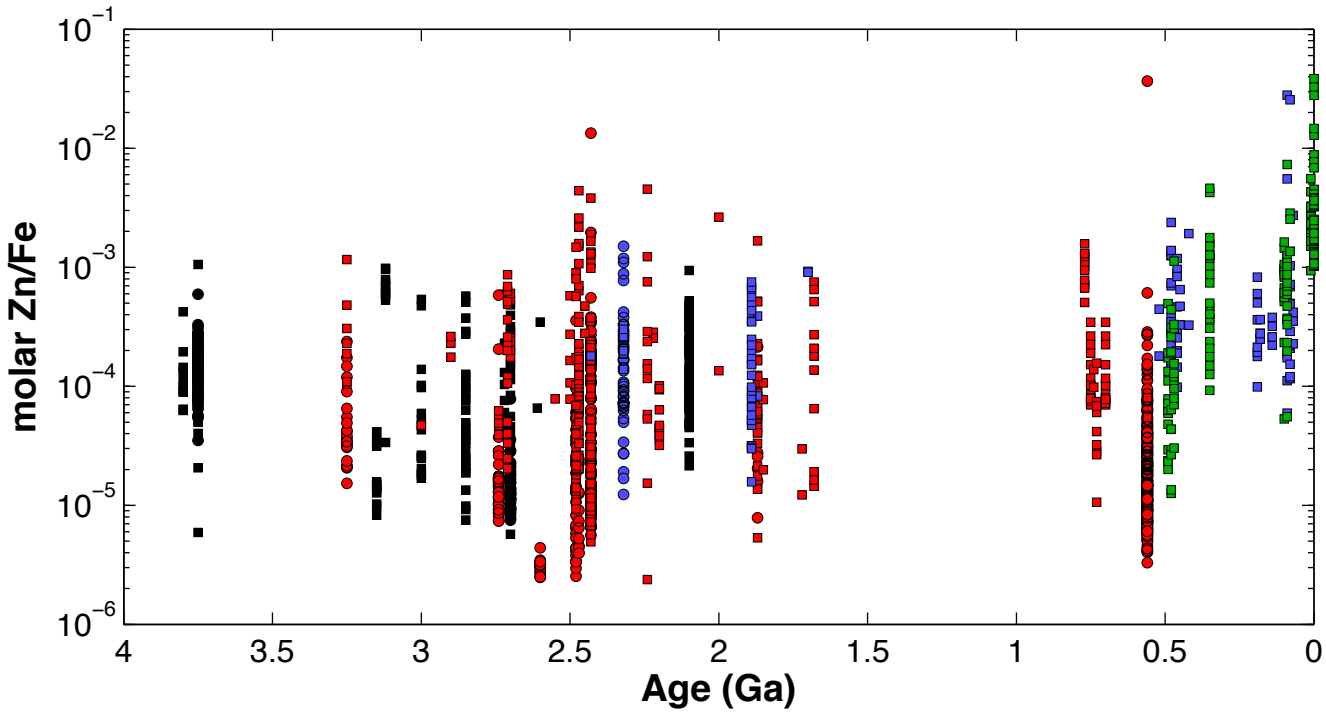
molar Zn/Fe
10^{-1}
10^{-2}
10^{-3}
10^{-4}
10^{-5}
10^{-6}
4
3.5
3
2.5
2
1.5
1
0.5
0
Age (Ga)

b)

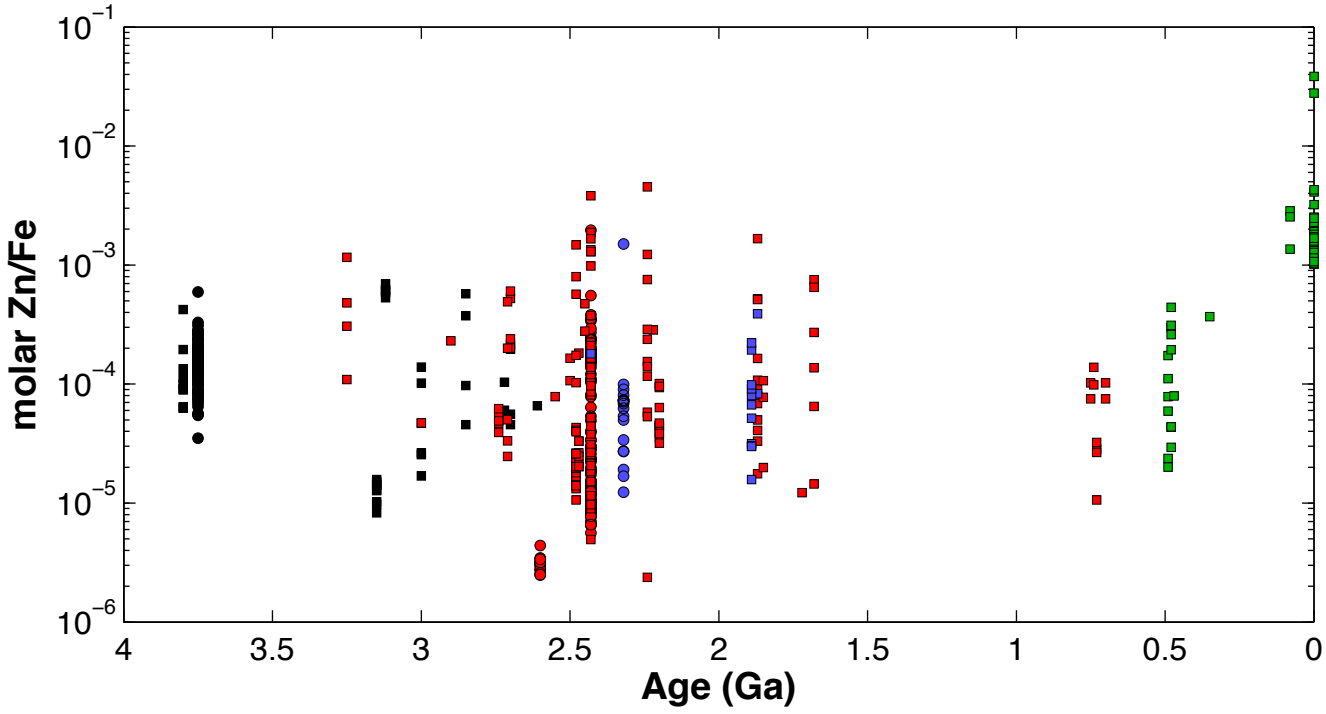
molar Zn/Fe
10^{-1}
10^{-2}
10^{-3}
10^{-4}
10^{-5}
10^{-6}
4
3.5
3
2.5
2
1.5
1
0.5
0
Age (Ga)

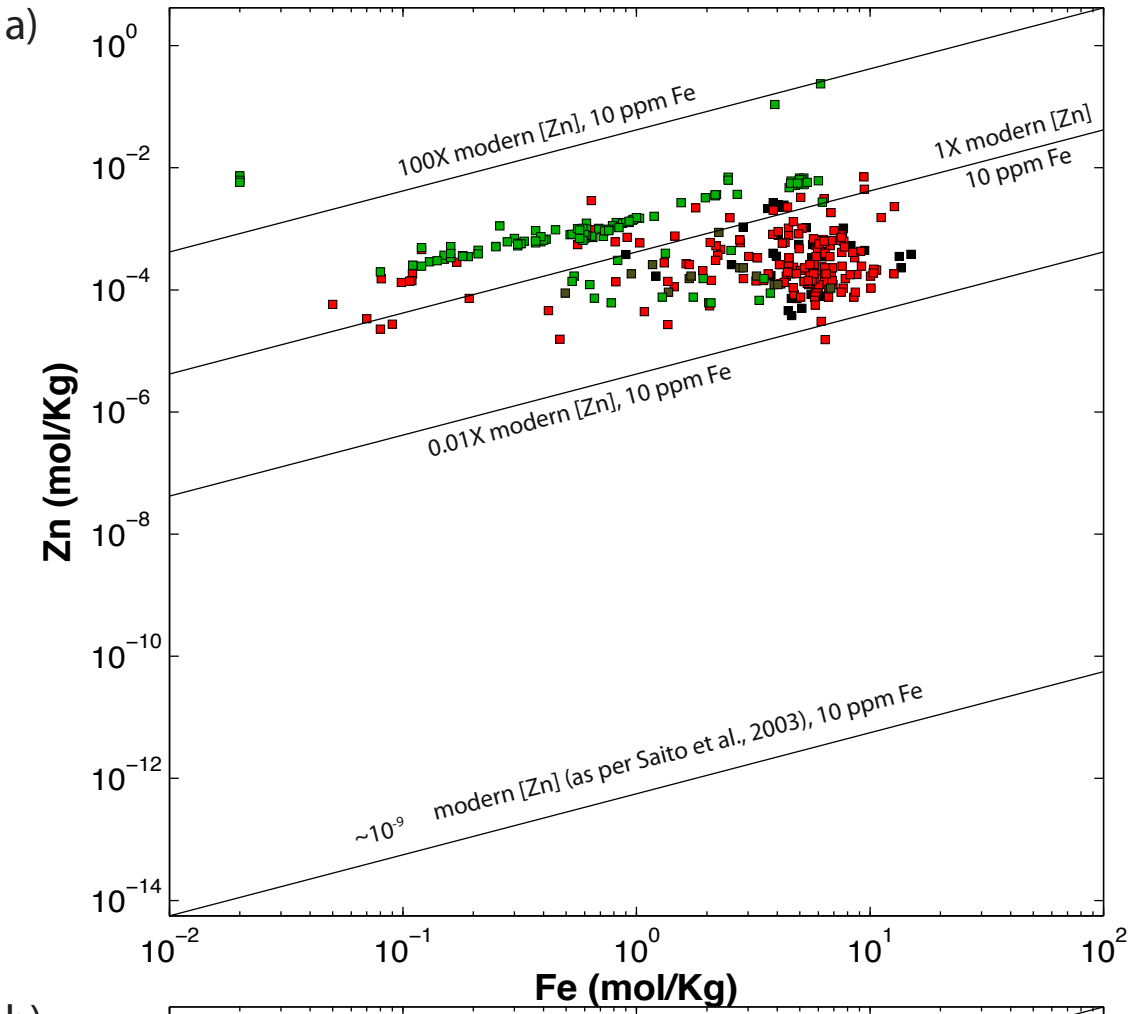
a)
100X modern [Zn], 10 ppm Fe
1X modern [Zn]
10 ppm Fe
0.01X modern [Zn], 10 ppm Fe
~10-9 modern [Zn] (as per Saito et al., 2003), 10 ppm Fe
Zn (mol/Kg)
Fe (mol/Kg)

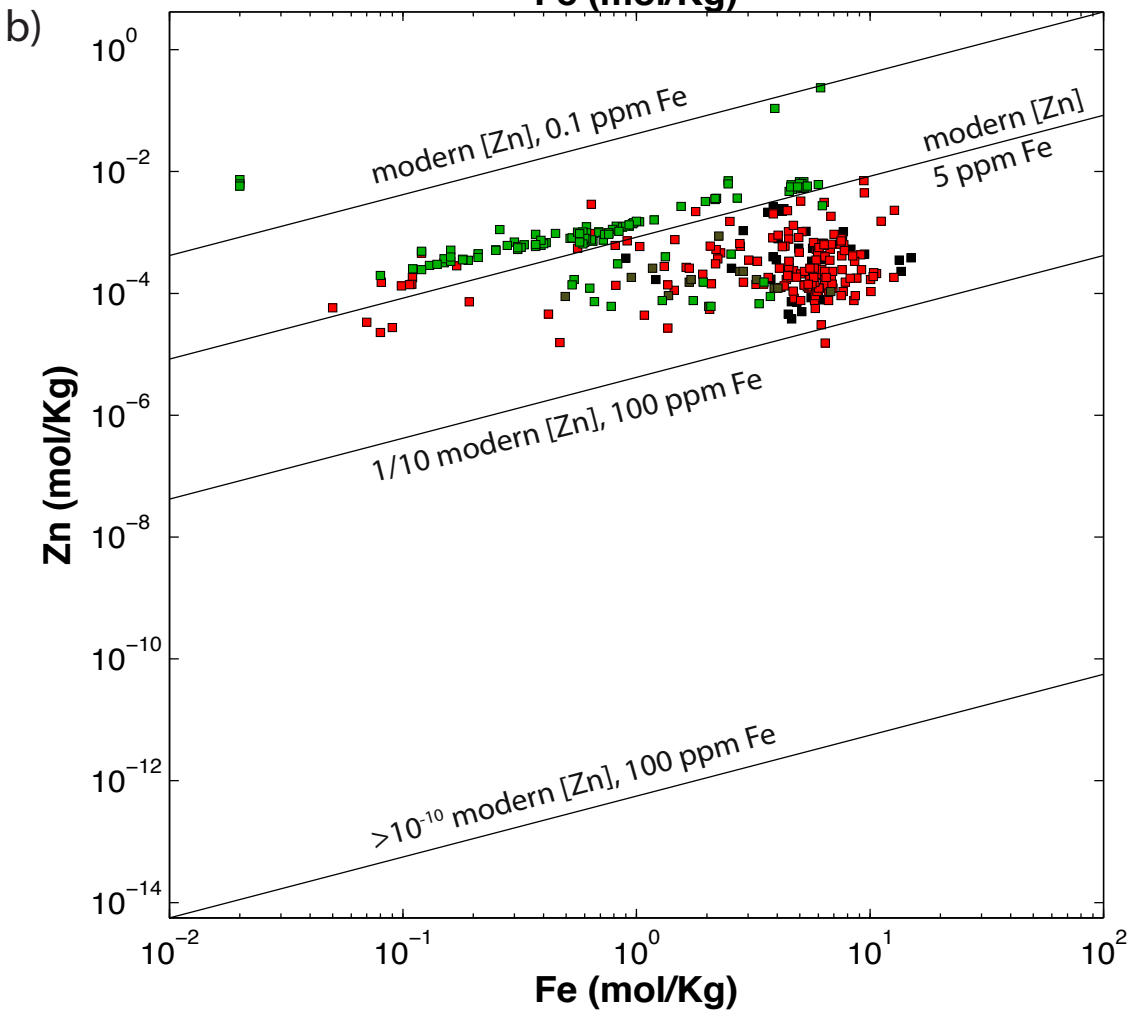
b)
modern [Zn], 0.1 ppm Fe
modern [Zn]
5 ppm Fe
1/10 modern [Zn], 100 ppm Fe
>10-10 modern [Zn], 100 ppm Fe
Zn (mol/Kg)
Fe (mol/Kg)